Non-Darcian flow experiments of shear-thinning fluids through rough-walled rock fractures

Antonio Rodríguez de Castro[1,2] and Giovanni Radilla[1,3]

[1]Arts et Métiers ParisTech, Châlons-en-Champagne, France, [2]Laboratoire MSMP-EA7350, Châlons-en-Champagne, France, [3]LEMTA, UMR 7563, CNRS, Vandœuvre-lès-Nancy, France

Key Points:
- Shear-thinning non-Darcian flow in rough fractures can be predicted from Newtonian flow and Darcian flow experiments with shear-thinning fluids
- Ours results apply for all the tested polymer concentrations of the used xanthan gum aqueous solutions
- For the first time, inertial and shear contributions to pressure loss have been identified for shear-thinning flow in fractures

Correspondence to:
A. Rodríguez de Castro,
antonio.rodriguezdecastro@ensam.eu

Abstract Understanding non-Darcian flow of shear-thinning fluids through rough-walled rock fractures is of vital importance in a number of industrial applications such as hydrogeology or petroleum engineering. Different laws are available to express the deviations from linear Darcy law due to inertial pressure losses. In particular, Darcy's law is often extended through addition of quadratic and cubic terms weighted by two inertial coefficients depending on the strength of the inertia regime. The relations between the effective shear viscosity of the fluid and the apparent viscosity in porous media when inertial deviations are negligible were extensively studied in the past. However, only recent numerical works have investigated the superposition of both inertial and shear-thinning effects, finding that the same inertial coefficients obtained for non-Darcian Newtonian flow applied in the case of shear-thinning fluids. The objective of this work is to experimentally validate these results, extending their applicability to the case of rough-walled rock fractures. To do so, flow experiments with aqueous polymer solutions have been conducted using replicas of natural fractures, and the effects of polymer concentration, which determine the shear rheology of the injected fluid, have been evaluated. Our findings show that the experimental pressure loss-flow rate data for inertial flow of shear-thinning fluids can be successfully predicted from the empirical parameters obtained during non-Darcian Newtonian flow and Darcian shear-thinning flow in a given porous medium.

1. Introduction

Non-Darcian flow through rough-walled rock fractures are of vital importance in numerous industrial applications such as geothermal energy production, CO_2 underground storage, and oil recovery [*Radilla et al*., 2013; *Tosco et al*., 2013]. In particular, shear-thinning fluids are commonly used in petroleum engineering and soil remediation to stabilize the injection front through mobility reduction. Injection of a shear-thinning fluid into a heterogeneous subsurface induces cross flow between higher and lower-permeability layers. Mobility reduction behind the polymer solution in a higher-permeability layer then creates a transverse pressure gradient that promotes fluid migration into less permeable layers [*Silva et al*., 2012]. Also, a number of fracturing fluids used in hydraulic fracturing present shear-thinning behavior, so knowledge of the flow rate-pressure gradient relationships is most valuable [*Lavrov*, 2015; *Perkowska et al*., 2016]. Most shear-thinning fluids used in remediation studies contained the biopolymer xanthan [*Zhong et al*., 2008; *Truex et al*., 2015]. Other polymers such as Carboxymethylcellulose [*Zhang et al*., 2016] and guar gum [*Hernández-Espriú et al*., 2013] are also widely used in drilling fluids for enhanced hydrocarbon recovery. Motivated by the wide range of industrial applications in which understanding non-Darcian flow of shear-thinning fluids is of key importance, the objective of the present work is to investigate the effects of the shear rheology of the injected fluid on the pressure losses generated during single-phase flow through fractures. In order to achieve this goal, a series of experiments are presented in which aqueous solutions of xanthan biopolymer with different polymer concentration are injected through two replicas of rough-walled natural fractures (granite and Vosges sandstone).

Darcy's law [*Darcy*, 1856] is generally used to model single-phase flow of incompressible Newtonian fluids through porous media. Nevertheless, this model is only valid when inertial forces are negligible compared to viscous forces [*Schneebeli*, 1955; *Hubbert*, 1956; *Scheidegger*, 1960; *Chauveteau and Thirriot*, 1967]. Both theoretical and empirical models taking into account the extra pressure losses due to inertial effects were

presented in previous works [*Miskimins et al*., 2005]. In particular, two different inertial regimes were identified: the strong inertial regime and the weak inertial regime. Forchheimer's empirical law [*Forchheimer*, 1901] is commonly used to model the strong inertial regime through addition of a quadratic pressure drop term to Darcy's law to describe the deviations from linearity:

$$-\frac{\Delta P}{L}=\frac{\mu}{K}\frac{Q}{A}+\beta\rho\left(\frac{Q}{A}\right)^2 \tag{1}$$

where $\frac{\Delta P}{L}$ is the pressure drop per unit of length, Q is the volumetric flow rate, μ the viscosity of the injected fluid, K is the intrinsic permeability, A is the cross-sectional area, ρ is the fluid density, and β is the inertial coefficient. Forchheimer's law has been experimentally validated [*Dullien and Azzam*, 1973; *Geertsma*, 1974; *MacDonald et al*., 1979; *Rasoloarijaona and Auriault*, 1994] and has found some theoretical justifications [*Cvetkovic*, 1986; *Giorgi*, 1997; *Chen et al*., 2001].

In the case of the weak inertial regime, which occurs at moderate values of the Reynolds number, deviations from the linear relationship between flow rate and pressure loss were shown to follow a cubic function of the mean velocity in the porous media [*Mei and Auriault*, 1991; *Firdaouss et al*., 1997; *Fourar et al*., 2004; *Rocha and Cruz*, 2010].

$$-\frac{\Delta P}{L}=\frac{\mu}{K}\frac{Q}{A}+\frac{\gamma\rho^2}{\mu}\left(\frac{Q}{A}\right)^3 \tag{2}$$

where γ is a dimensionless inertial coefficient. Reynolds number can be specifically defined for weak inertia cubic law as [*Radilla et al*., 2013].

$$Re_c=\sqrt{K\gamma}\frac{\rho}{\mu}\frac{Q}{A} \tag{3}$$

Cubic law was obtained from numerical simulations in a 2-D periodic porous medium [*Barrère*, 1990; *Firdaouss and Guermond*, 1995; *Amaral Souto and Moyne*, 1997] and also by using the homogenization technique for isotropic homogeneous porous media [*Mei and Auriault*, 1991; *Wodie and Levy*, 1991]. This law was shown to be in agreement with experimental data [*Firdaouss et al*., 1997]. *Fourar et al*. [2004] demonstrated that the transition zone between cubic and quadratic inertial deviations is reduced in the case of 3-D flows as those in granular media.

Using the asymptotic expansions method in a thin cylindrical channel with oscillating walls and averaging over the channel diameter, *Buès et al*. [2004] and *Panfilov and Fourar* [2006] presented a macroscopic flow equation which proved to be in good agreement with numerical simulations in rectangular and cylindrical fractures at high flow rates. This flow equation was expressed in the form of a full cubic law:

$$-\frac{\Delta P}{L}=\frac{\mu}{K}\frac{Q}{A}+\beta\rho\left(\frac{Q}{A}\right)^2+\frac{\gamma\rho^2}{\mu}\left(\frac{Q}{A}\right)^3 \tag{4}$$

where β and γ are the inertial coefficients which may be positive or negative, depending on the channel geometry. In this full cubic law, the quadratic term describes the pure inertia effect caused by an irreversible loss of kinetic energy due to flow acceleration and the cubic term corresponds to a cross viscous-inertia effect caused by the streamline deformation due to inertia forces. This macroscopic flow equation is valid not only in the Darcian flow regime but also, to some limited extent, for the non-Darcian flow regimes. Obtaining β and γ through fitting to experimental data is of valuable interest as it would permit comparison to previous theoretical predictions by oly obtained from porosity, permeability, and roughness of the porous medium [*Cornell and Katz*, 1953; *Geertsma*, 1974; *Neasham*, 1977; *Noman and Archer*, 1987; *López*, 2004, *Agnaou et al*., 2013; *Agnaou*, 2014].

Analogously to the case of cubic law, Reynolds number can be defined for full cubic law as [*Radilla et al*., 2013]:

$$Re_{fc}=K\beta\frac{\rho}{\mu}\frac{Q}{A} \tag{5}$$

Previous experimental works demonstrated that Darcy's law fails to predict pressure drops in fractures when inertial effects are relevant [*Zimmerman* et al., 2004; *Radilla et al*., 2013]. *Radilla et al*. [2013] modeled single-phase flow experiments by means of the full cubic law and presented an elegant method to compare

fractures in terms of hydraulic behavior versus flow regime using the intrinsic hydrodynamic parameters. Besides, a geometrical model for nonlinear fluid flow through rough fractures was proposed and evaluated through numerical simulations by *Javadi et al.* [2010]. Also, several authors showed that the intrinsic permeability K and the cross-sectional area A used in equations (1–5) can be written as functions of the hydraulic aperture of the fracture h [*Witherspoon et al.*, 1980; *Brown*, 1987; *Zimmerman and Yeo*, 2000; *Brush and Thomson*, 2003]:

$$K = \frac{h^2}{12} \tag{6}$$

$$A = hw \tag{7}$$

where w is the fracture width.

The specific objectives of the present study are to investigate how shear-thinning behavior affects the relationships between Reynolds number and pressure losses in fractures and validate previous numerical and theoretical predictions which stated the uniqueness of the inertial coefficients for a given porous medium, extending their applicability to the case of rough-walled rock fractures. To do so, flow experiments with aqueous polymer solutions have been conducted using replicas of natural fractures, and the effects of polymer concentration, which determine the shear rheology of the injected fluid, have been addressed. In this work, we first hypothesize that the differences between the pressure drops measured during the flow of the investigated shear-thinning fluids through rough-walled rock fractures and the pressure drop as predicted from the shear viscosity of the fluid can be explained in terms of inertial effects generated in the porous medium flow. This hypothesis is then validated through analysis of the experimental results.

2. Non-Darcian Flow of Shear-Thinning Fluids in Porous Media

The use of Newtonian assumption in equations (1–5) is not realistic in the case of shear-thinning fluids, leading to important errors. Indeed, μ depends on Q for these fluids, so this relationship must be included in the mentioned equations. In addition, although numerical and theoretical studies have stated that the inertial coefficients β and γ do not depend on the fluid rheology, no experimental evidence has been presented. In particular, *Tosco et al.* [2013] demonstrated through numerical experiments that the value of the inertial parameter β is independent of the viscous properties of the fluid. Also, γ was analytically and numerically shown to be a porosity-dependent parameter by *Firdaouss et al.* [1997] and by *Yazdchi and Luding* [2012]. Therefore, experimental validation of these results is most valuable. A potential experimental issue concerns elongational flows, which are known to induce extra pressure losses as compared to those predicted by pure shear flow during the injection of solutions of polymers presenting a certain degree of flexibility through changing cross-sectional area media such as porous media [*Rodríguez et al.*, 1993; *Müller and Sáez*, 1999; *Nguyen and Kausch*, 1999; *Seright et al.*, 2011; *Amundarain et al.*, 2009]. This was attributed to the formation of transient entanglements of polymer molecules due to the action of the extensional component of the flow. Measurement of extensional viscosity is tricky and several methods have been proposed for its determination [*Schunk et al.*, 1990; *Petrie*, 2006; *Collier et al.*, 2007]. One of the simplest methods consists in the use of an opposed-jet device [*Willenbacher and Hingmann*, 1994; *González et al.*, 2005]. However, important differences between the results obtained by the available methods were reported [*Petrie*, 2006].

The empirical Carreau model [*Carreau*, 1972] is one of the most popular models to represent the shear-thinning behavior of semidilute polymer solutions [*Sorbie et al.*, 1989; *López et al.*, 2003; *Rodríguez de Castro et al.*, 2016] commonly used in Enhanced Oil Recovery (EOR) and soil remediation. The Carreau equation is based on molecular network theory and is often presented as $\frac{\mu-\mu_\infty}{\mu_0-\mu_\infty} = \left[1+(\lambda\dot{\gamma})^2\right]^{\frac{n-1}{2}}$, where μ is the viscosity at a given shear rate $\dot{\gamma}$, μ_0 and μ_∞ are the zero shear rate and infinite shear rate viscosities, respectively, n is the power-law index, and λ is the time constant. The values of μ_0, μ_∞, n, and λ are determined by the polymer concentration under given pressure and temperature conditions. In the region far from the low shear viscosity plateau, i.e., when $\dot{\gamma} \gg \frac{1}{\lambda}$, Carreau's law leads to the following expression:

$$\mu \approx \mu_\infty + (\mu_0-\mu_\infty)\lambda^{n-1}\dot{\gamma}^{n-1} = \mu_\infty + a\dot{\gamma}^{n-1} \tag{8}$$

with $a = (\mu_0-\mu_\infty)\lambda^{n-1}$. From this expression, it can be observed that all the combinations of μ_0 and λ providing the best fit to a set of μ versus $\dot{\gamma}$ experimental data will result in the same value of the parameter a in

the case in which no experimental data are available within the low shear rate viscosity plateau. Therefore, the actual values of μ_0 and λ cannot be properly determined in this case.

The importance of inertial effects in the porous medium can be quantified through comparison of the calculated shear viscosity to the actually observed equivalent viscosity. The equivalent viscosity in the porous medium μ_{eq} is defined as the quantity that must replace the viscosity in Darcy's law to result in the same pressure drop actually measured [*Tosco et al*., 2013]. Indeed, both inertial and shear-thinning effects are encompassed in μ_{eq}. In the case of a rectangular fracture, μ_{eq} is expressed as:

$$\mu_{eq} = -\frac{\nabla P}{Q} KA = -\frac{\nabla P}{Q}\frac{h^3 w}{12} \tag{9}$$

The apparent shear rate in the porous medium has to be determined in order to calculate the "in situ" shear viscosity μ_{pm}. The apparent shear rate $\dot{\gamma}_{pm}$ of shear-thinning fluids flowing through a porous medium can be defined by dividing the mean velocity Q/A by a characteristic microscopic length of the porous media [*Chauveteau*, 1982; *Sorbie et al*., 1989; *Perrin et al*., 2006; *Tosco et al*., 2013; *Rodríguez de Castro et al*., 2016]. This microscopic length is usually taken as $\sqrt{K\varepsilon}$ with ε being the porosity of the porous medium. From the definition of cross-sectional area (equation (7)), it is expected that in the particular case of fractures the porosity is close to unit. Therefore, $\dot{\gamma}_{pm}$ can be defined as:

$$\dot{\gamma}_{pm} = \alpha\frac{\frac{Q}{A}}{\sqrt{K}} = \alpha\frac{Q\sqrt{12}}{h^2 w} \tag{10}$$

where α is a empirical shift factor known to be a function of both the bulk rheology of the fluid and the porous media [*Chauveteau*, 1982; *López et al*., 2003; *López*, 2004; *Comba et al*., 2011; *Sorbie et al*., 2013]. Consequently, in the case of Carreau fluids flowing at moderate and high shear rates μ_{pm} can be obtained from equation s (8) and (10):

$$\mu_{pm} = \mu_\infty + a\left(\alpha\frac{Q\sqrt{12}}{h^2 w}\right)^{n-1} \tag{11}$$

3. Materials and Methods

3.1. Experimental Setup and Procedure

A set of experiments was conducted injecting aqueous polymer solutions through transparent epoxy resin replicas of natural rough-walled rock fractures. The original fractures used in this work are a Vosges sandstone sample with dimensions 26 cm long and w = 14.8 cm wide, and a granite sample with dimensions 33 cm long and w = 15.5 cm wide. Details of the fabrication process of these fracture replicas can be found elsewhere [*Isakov et al*., 2001; *Nowamooz et al*., 2013]. The aperture maps of the fractures were determined using the image processing procedure based on the attenuation law of Beer-Lambert presented by *Nowamooz et al*. [2013] and *Radilla et al*. [2013]. These aperture maps have been included as supporting information Figures S1 and S2 and are referenced in the text of the present article. Both aperture maps clearly show high spatial variability of the fracture aperture fields. For both fractures, smaller apertures are located at the center and the larger apertures are located near the inlet and the outlet of the fractures. The lower half of the Vosges sandstone fracture aperture field shows higher variability than the upper half, while for the granite fracture, the spatial variability appears to be relatively high across the entire fracture area. A detailed analysis of the aperture variability and distribution in both fractures was performed by *Nowamooz et al*. [2013]. As explained by these authors, granite fracture aperture field is more variable (heterogeneous) than the Vosges sandstone one. Also, the authors shown that the spatial variability of the fracture aperture field, especially the constricted areas at the center of the fractures, was shown to result in the creation preferential paths for the flow of the fluid. These effects are expected to be more important in the case of shear-thinning fluids as the pressure loss sensitivity to aperture is higher (shear viscosity depends on the local aperture).

The fluid was injected from a tank situated upstream of the fracture using a volumetric pump (EcoMoineau M Series, PCM, France), and its flow rate was measured with a positive displacement flow meter (Model LSM45, Oval, Japan). A differential pressure sensor (DP15 Variable Reluctance Pressure Sensor, Validyne,

USA) was used to measure the pressure drop over a distance of L = 20.5 cm in the case of the Vosges sandstone fracture and L = 27 cm in the case of the granite fracture. The injected fluid was continuously recirculated to the upstream tank after passing through the fracture. A sketch of the experimental setup is included as supporting information Figure S3.

The procedure followed in our experiments was similar to the one used in the single-phase flow experiments conducted by *Radilla et al.* [2013]. In this procedure, the fractures were saturated with CO_2 prior to saturation with polymer solution in order to avoid generation of air bubbles. Once saturated with polymer solution, a set of 26 different flow rates ranging from 9 to 250 L/h were imposed for the flow through the fracture and the corresponding steady state pressure drops were measured. The room temperature was kept constant at 18°C ± 1.

3.2. Fluid Properties

Four xanthan gum aqueous solutions with polymer concentrations C_p of 0, 200, 500, and 700 ppm were used as injected fluids in the present experiments. Xanthan gum is a commonly used viscosifier obtained through fermentation of Xanthomonas campestris bacteria [*Garcia-Ochoa et al.*, 2000; *Palaniraj and Jayaraman*, 2011; *Wadhai and Dixit*, 2011]. In solution state, an isolated xanthan macromolecule is more or less rigid and is of typically 1 μm of contour length [*Mongruel and Cloitre*, 2003] and a transverse size of approximately 2 nm. Additional information about its chemical composition, structure, and other physicochemical properties can be found elsewhere [*Song*, 2007].

Each solution of 60 L were prepared by dissolving xanthan gum in filtered water containing 400 ppm of NaN_3 as a bactericide. The xanthan gum powders were progressively dissolved in water while gently mixing with a custom-made overhead device. Once prepared, the polymer solutions were characterized by means of a stress-controlled rheometer (ARG2, TA Instruments) equipped with cone-plate geometry at a constant temperature of 18°C ± 1, following a procedure previously presented in the literature [*Rodríguez de Castro*, 2014; *Rodríguez de Castro et al.*, 2014]. Viscosity measurements at very low shear rates were not possible with the used equipment due to the difficulty to reach steady state values with rotational rheometers at very low shear rates in the case of low viscosity fluids as the used solutions [*Hallouche et al.*, 2015]. However, this is not important in the case of the present experiments as the involved viscosity values are far from the low shear rates viscosity plateau. A viscosity of 0.0011 Pa s was measured for the solvent (water) and the density ρ of all injected fluids was taken as 1000 kg/m^3. Moreover, a set of effluent fluid samples were collected at the outlet of the fractures after injection at the highest flow rate. The effluent rheograms were determined and compared to that of the inflowing fluid in order to assess polymer degradation and retention of the polymer on the fracture walls. No significant difference was observed between the rheograms, so polymer degradation and significant polymer retention were proved to be negligible.

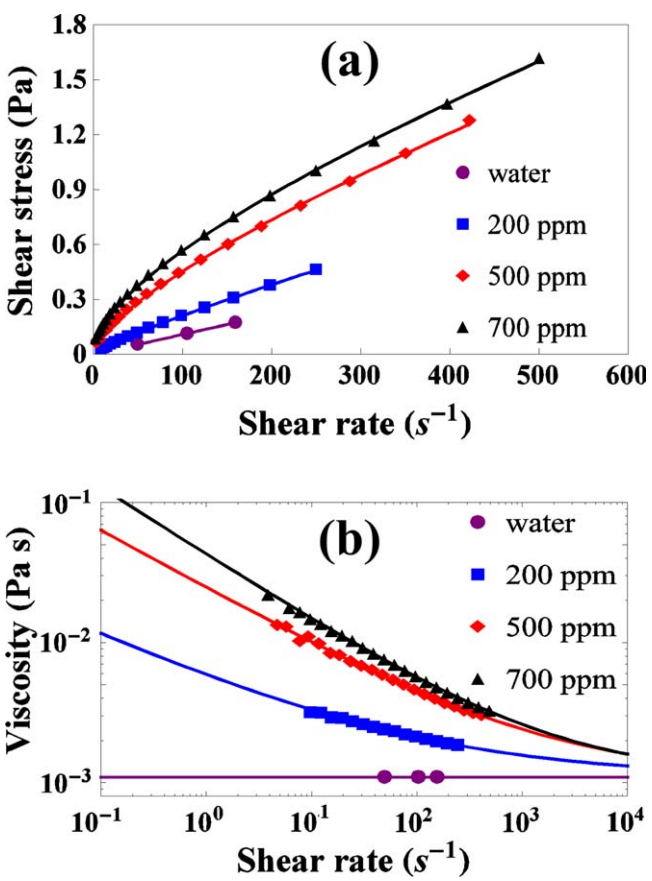

Figure 1. (a) Rheograms and (b) effective viscosity versus shear rate for the polymer concentrations of the injected fluid. The symbols represent experimental data and solid lines represent the fitted curves using the equation (8).

Table 1. Parameters Used in Equation (8) for the Shear Rate-Viscosity Relations Shown in Figure 1b

C_p (ppm)	a (Pa s^n)	μ_∞ (Pa s)	n
200	4.8×10^{-3}	1.1×10^{-3}	6.6×10^{-1}
500	2.4×10^{-2}	1.1×10^{-3}	5.8×10^{-1}
700	4.2×10^{-2}	1.1×10^{-3}	5.2×10^{-1}

The empirical Carreau model [*Carreau*, 1972] is commonly used to represent the shear-thinning behavior of xanthan gum semidilute solutions [*Sorbie et al*., 1989; *López et al*., 2003; *Rodríguez de Castro et al*., 2016]. All the viscosity values involved in the present experiments are far from the low shear rate plateau. For this reason, equation (8) will be used to fit the viscosity measurements. However, viscosity measurements must be performed within the low shear rate pleateau in order to determine the values of μ_0 and λ in the applications in which flow at very low shear rates is involved.

Equation (8) was used to fit the experimental data shown in Figure 1, and the obtained values for a and n are presented in Table 1. μ_∞ was assumed to be that of the solvent, which is supported by previous studies [*Bird et al*., 1987; *Pauchard et al*., 1999; *López*, 2004; *Saggin and Coupland*, 2004; *Auradou et al*., 2008; *Comba et al*., 2011; *Wengeler*, 2014; *Fang et al*., 2015].

From Figure 1b, it can be deduced that higher viscosities are obtained for high values of C_p and that the experimental data are well described by equation (8). The data in Table 1 illustrate that the zero shear rate viscosity of xanthan gum solutions increase with increasing C_p, while parameter a decreases. Besides, the value of n decreases with increasing C_p, reflecting that the shear-thinning behavior is more pronounced at higher C_p.

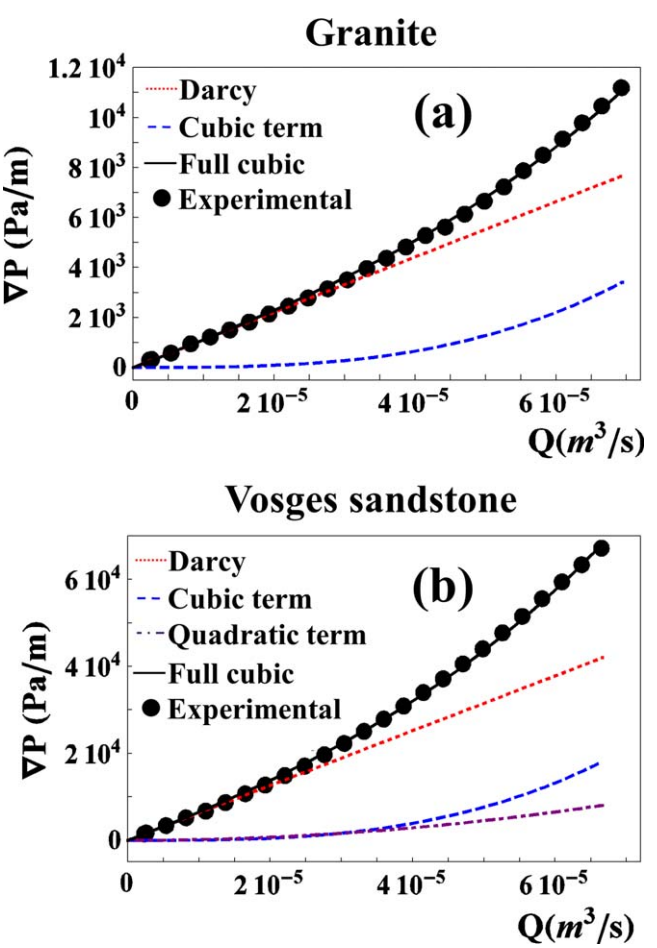

Figure 2. Pressure gradient versus flow rate for water injection through the (a) granite fracture and (b) Vosges sandstone fracture. Symbols represent experimental data, black solid lines represent their fit to a cubic law, red-dotted lines represent the linear term (Darcy's law), blue-dashed lines represent the contribution of the quadratic term to the full cubic law fit, and purple dot-dashed lines represent the contribution of the cubic term to the full cubic law fit.

4. Results and Discussions

The flow experiments were conducted for all four polymer concentrations and were repeated four times. For each concentration, a total of a 104 measurements (4 repetitions for each of the 26 flow rates) were completed. The 104 measures for a given polymer concentration-fracture pair were considered to be an experimental set.

4.1. Non-Darcian Flow of a Newtonian Fluid: Obtaining K, γ, and β From Experiments

The experimental sets of pressure gradient as a function of Q for water injection ($C_p = 0$ ppm) through both fractures are presented in Figure 2. Directly fitting the third-order polynomial to the whole set of data would result in overestimation of permeability [*Du Plessis and Masliyah*, 1988; *Dukhan et al*., 2014]. Indeed, by fitting the whole set of data to the polynomial law, a part of the pressure drop would be attributed to inertial effects even at the lowest flow rates, which is not realistic. Consequently, the viscous pressure loss would be underestimated leading to permeability overestimation. To avoid this issue, h and K are determined by following a two-steps procedure:

Table 2. Permeability and Inertial Coefficients (Equation (4)) of the Used Fractures[a]

Fracture	h (m)	K (m^2)	γ	β (m^{-1})
Granite	9.10×10^{-4} ($\pm$1%)	6.90×10^{-8} ($\pm$2%)	3.25×10^{-5} ($\pm$3%)	0
Vosges sandstone	5.19×10^{-4} ($\pm$2%)	2.25×10^{-8} ($\pm$4%)	3.03×10^{-5} ($\pm$5%)	10.7 ($\pm$2%)

[a]Percentages represent relative standard deviation.

1. In this step, the hydraulic apertures h_j obtained by only using the first j experimental data (starting with the lowest flow rates) are calculated by minimizing the sum $\sum_{i=1}^{j}\left(\nabla P_i - \frac{12Q_i\mu}{h_j^3 w}\right)^2$ for $j = 1...N$, with N being the number of experimental data and μ being the measured dynamic viscosity of water at the room temperature (0.0011 Pa s).
2. Then, the quality of N fits obtained by using the N values of h_j calculated in the preceding step is evaluated by using the merit function $F(j) = \frac{\sum_{i=1}^{j}\left|\frac{\nabla P_i - \frac{12Q_i\mu}{h_j^3 w}}{\nabla P_i}\right|}{j}$ for $j = 1...N$. After that, the value of j minimizing $F(j)$ was determined. The corresponding h_j value was selected as the hydraulic aperture of the fracture from which K was calculated using equation (6). The obtained values of K and h are presented in Table 2.

Once permeability was determined, the $(Q_i, \nabla P_i,)$ data were fitted to a full cubic law (equation (4)) through a standard least squares method using the value of K calculated in the previous step and obtaining the values for γ and β, which are also listed in Table 2.

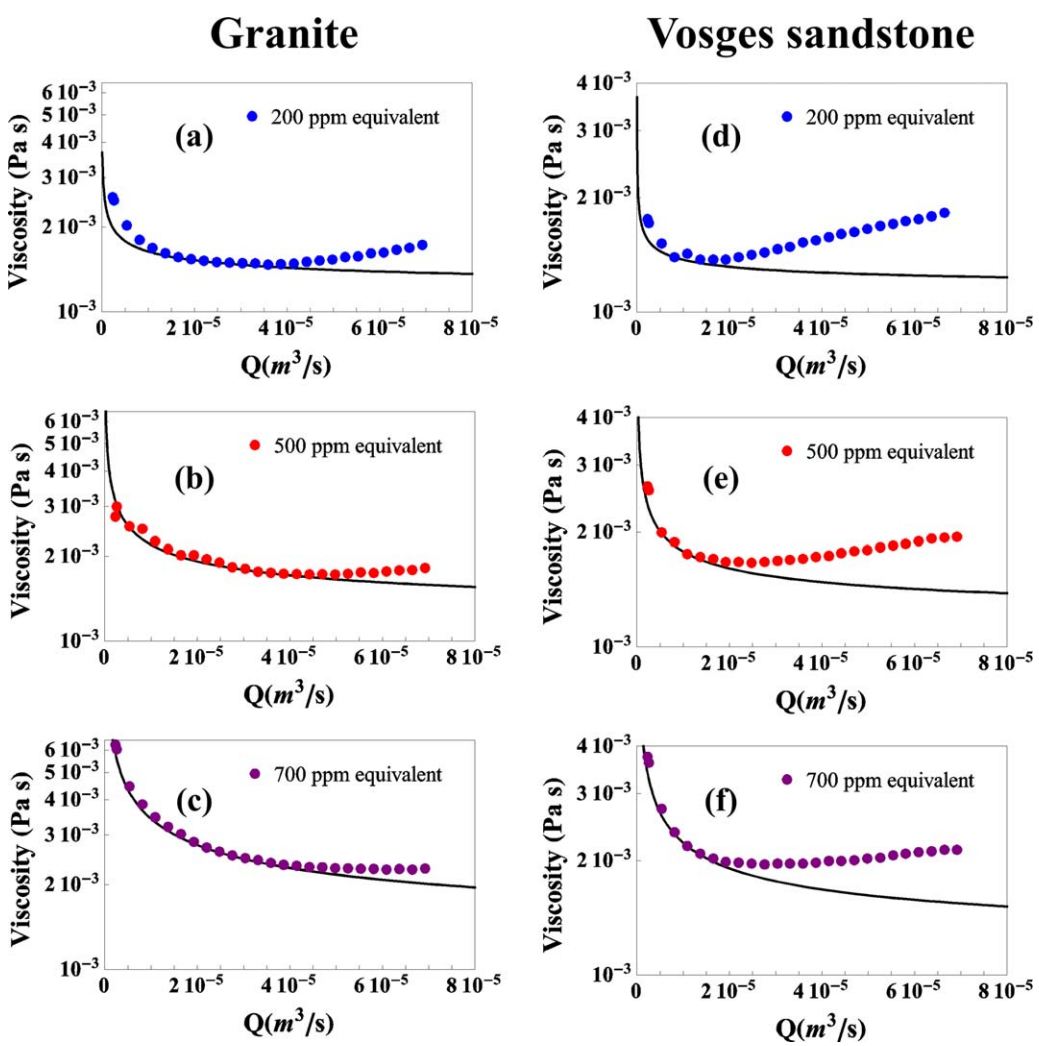

Figure 3. μ_{eq} and μ_{pm} for the polymer concentrations of the injected fluid. Symbols represent μ_{eq} and solid lines represent μ_{pm}. (a), (b), and (c) Correspond to the granite fracture. (d), (e), and (f) Correspond to the Vosges sandstone fracture.

Table 3. Apparent-to-Effective Viscosity Shift Factor α for the Used Fractures and Fluids

C_p (ppm)	α (Granite Fracture)	α (Vosges Sandstone Fracture)
200	2.4	5.4
500	5.7	5.5
700	1.5	2.1

4.2. Equivalent and Shear Viscosity Relations

In our experiments, α was determined for each porous medium-fluid pair by overlaying the porous medium μ_{eq} versus $\dot{\gamma}_{app}$ with the bulk μ_{eq} versus $\dot{\gamma}$ curves as closely as possible and noting the scale change in shear rate required to obtain the best fit. This criterion to select α was proposed by *Sorbie et al.* [1989] as a pragmatic alternative to the original one previously proposed by *Chauveteau* [1982], and was subsequently used by other authors [*González et al.*, 2005; *Amundarain et al.*, 2009]. It should be noted that a good overlay between both curves is only possible in the low flow rates region where no significant inertial effects occur, as shown in Figure 3. The obtained values for α are given in Table 3. It is observed that all values lie in the interval 1–15, in agreement with literature data [*Chauveteau*, 1982; *Sorbie et al.*, 1989; *López et al.*, 2003; *Comba et al.*, 2011]. Moreover, μ_{pm} predicted from rheological measurements in the rheometer overlaps μ_{eq} in the low flow rates region, showing that the effect of fluid-solid interactions (e.g., polymer mechanical degradation and apparent wall slip) on the relationship between viscosity and shear rate is negligible [*González et al.*, 2005; *Amundarain et al.*, 2009; *Rodríguez de Castro et al.*, 2016].

4.3. Polymer Concentration Effects on Reynolds Number

While Reynolds number is directly proportional to injection flow rate for Newtonian fluids, this is not the case when using shear-thinning fluids. Indeed, according to equation s (10) and (11), increasing the flow rate implies a decrease in viscosity which implies in turn an extra increase in Reynolds number. The Reynolds numbers obtained for the imposed flow rate were calculated through equation (3) in the case of the granite fracture and equation (5) in the case of the Vosges sandstone fracture. μ_{pm} was used for the calculation of Reynolds number. It is highlighted that μ_{pm} accounts only for viscous effects and consistent with the definition of Reynolds number as the ratio of inertial to viscous forces, in contrast to μ_{eq}. The results

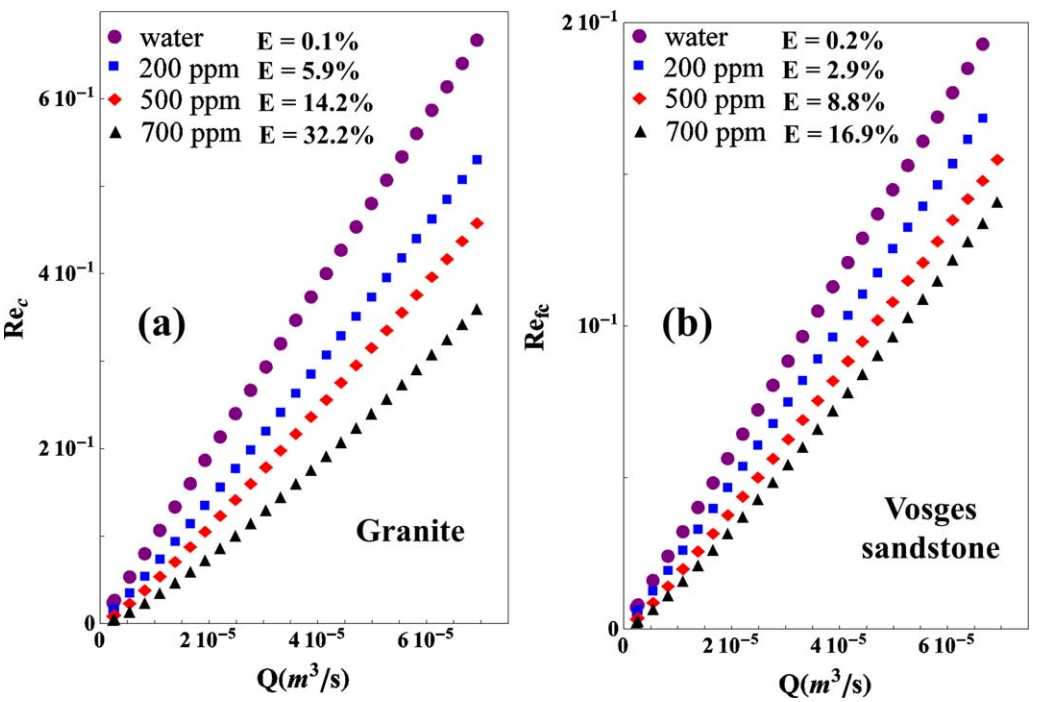

Figure 4. (a) Re_c versus Q for the granite fracture (b) Re_{fc} versus Q for the Vosges sandstone fracture. The average relative error E of a linear fit is presented in each case.

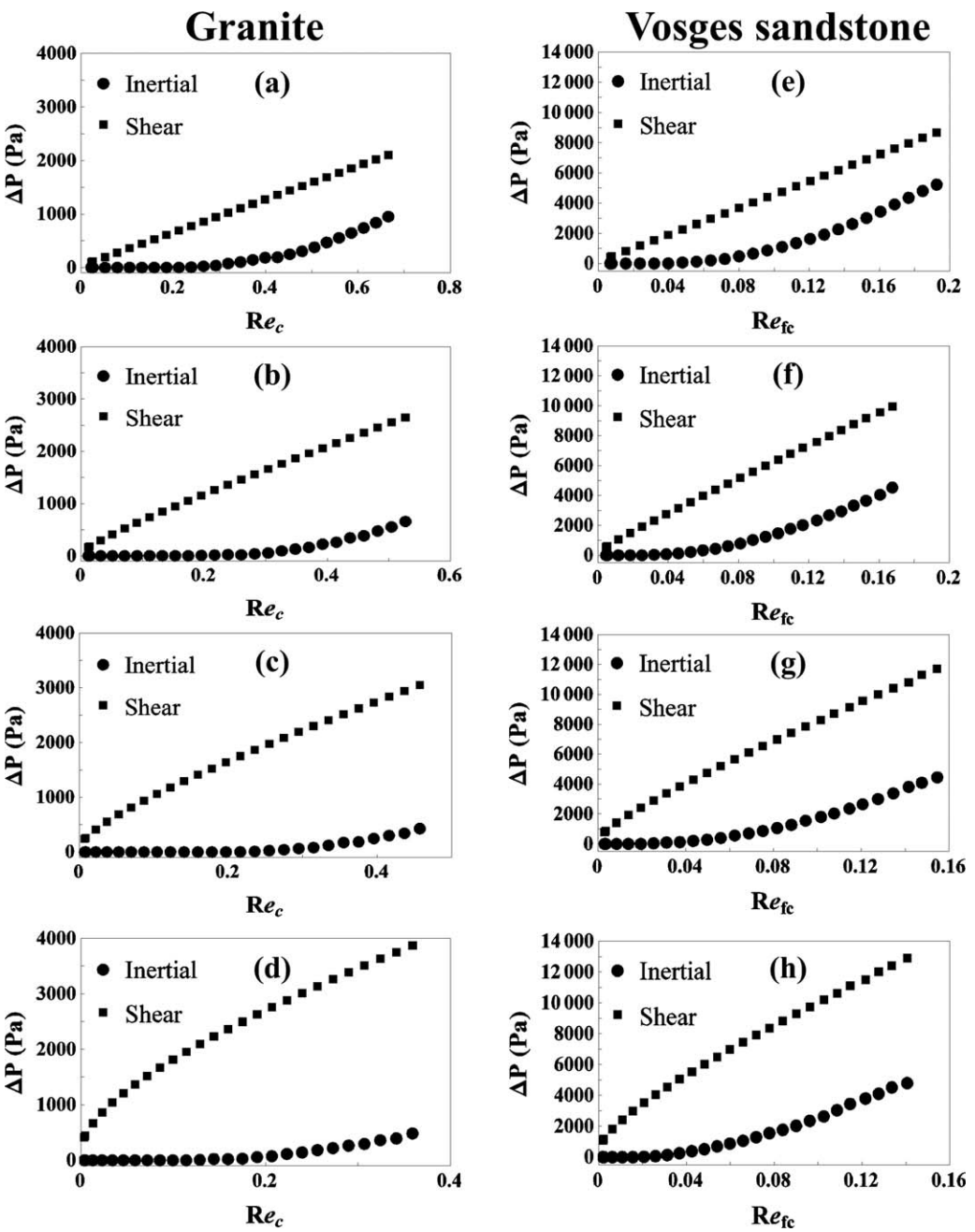

Figure 5. Pressure losses due to shear and inertial dissipation as a function of Re_c and Re_{fc} corresponding to (a) Granite – water, (b) Granite – 200 ppm solution, (c) Granite – 500 ppm solution, (d) Granite – 700 ppm solution, (e) Vosges – water, (f) Vosges – 200 ppm solution, (g) Vosges – 500 ppm solution, and (h) Vosges – 700 ppm solution.

are presented in Figure 4. In this figure, it can be observed that Reynolds number decreases as C_p increases for a given flow rate. Also the range of Reynolds numbers corresponding to the range of imposed flow rates is narrower as C_p increases. This was expected given the higher viscosity values of the most concentrated solutions.

Moreover, the average relative errors E resulting from the fit of Reynolds as a function of Q using a linear model were calculated in each case as $E = \frac{\sum_{j=1}^{N} \frac{|\text{fit}(Q_j) - \text{Reynolds}_j|}{\text{Reynolds}_j}}{N}$, with N being the number of experimental data. These average errors are shown in Figure 4 for both fractures.

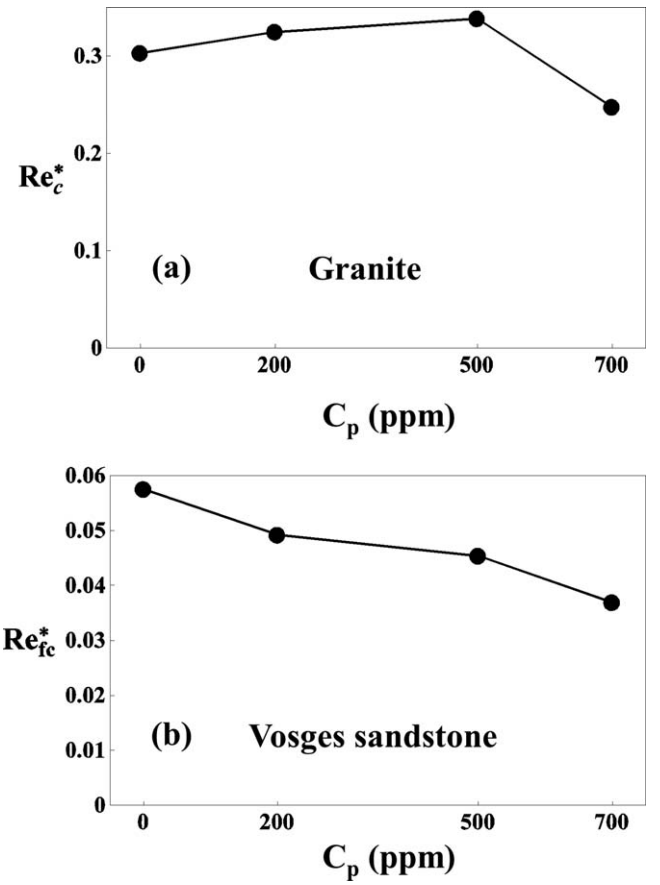

Figure 6. Critical Reynolds numbers versus polymer concentration for (a) Granite and (b) Vosges sandstone fractures.

4.4. Extension of Weak Inertia Cubic Law and Full Cubic Law to Shear-Thinning Fluids

The total pressure loss through the fracture ΔP_{total} results from the superposition of two contributions [*González et al.*, 2005; *Tosco et al.*, 2013], one of them ΔP_{shear} being strictly related to the shear viscosity of the shear-thinning fluid and the other one $\Delta P_{inertial}$ being related to the inertial effects arising at high flow rates:

$$\Delta P_{total} = \Delta P_{shear} + \Delta P_{inertial} \tag{12}$$

The shear contribution to the pressure loss can be expressed from Darcy's law as follows:

$$-\Delta P_{shear} = \frac{\mu_{pm} Q}{KA} L \tag{13}$$

where μ_{pm} is the porous medium viscosity as defined by equation (11).

On the other hand, the inertial contribution to the pressure loss is obtained from the nonlinear terms of equation (4) and is expressed as:

$$-\Delta P_{inertial} = \beta\rho\left(\frac{Q}{A}\right)^2 L + \frac{\gamma\rho^2}{\mu_{pm}}\left(\frac{Q}{A}\right)^3 L \tag{14}$$

$\Delta P_{inertial}$ and ΔP_{shear} were calculated and presented in Figure 5 as a function of Reynolds number and C_p for both fractures. It is noted that μ used in the definition of Reynolds number, i.e., in equations (3) and (5), has been taken as being the viscosity of the solvent in previous works [*González et al.*, 2005; *Amundarain et al.*, 2009]. However, as shown in the preceding subsection, shear-thinning behavior has an important effect on the range and values of Reynolds number. Consequently, in the present work μ_{pm} was used in in equations (3) and (5) instead of water viscosity.

Figure 5 shows that $\Delta P_{inertial}$ is negligible below a certain value of Reynolds number, i.e., within the shear-thinning Darcy regime. Two types of criteria, the Reynolds number and the Forchheimer number, have been proposed in the literature to identify the onset of non-Darcian flow. A review on these criteria was presented by *Zeng and Grigg* [2006]. In the present study, the critical value of Reynolds number, named Re_c^* for the granite fracture (cubic law) and Re_{fc}^* for the Vosges sandstone fracture (full cubic law), will be defined as being the one for which $\Delta P_{inertial}$ is approximately 5% of ΔP_{total}. Consequently, inertial effects will be considered to be significant only above this critical Reynolds number. Re_c^* and Re_{fc}^* were calculated for the granite and the Vosges sandstone fractures, respectively, for all values of C_p considered and the results are presented in Figure 6.

For a full cubic law, the pressure gradient during the flow of shear-thinning fluids is given by combination of equations (4) and (11):

$$-\frac{\Delta P}{L} = \frac{\mu_{pm}}{K}\frac{Q}{A} + \beta\rho\left(\frac{Q}{A}\right)^2 + \frac{\gamma\rho^2}{\mu_{pm}}\left(\frac{Q}{A}\right)^3 \tag{15}$$

with $\beta = 0$ in the particular case of weak inertia regime (for the granite fracture).

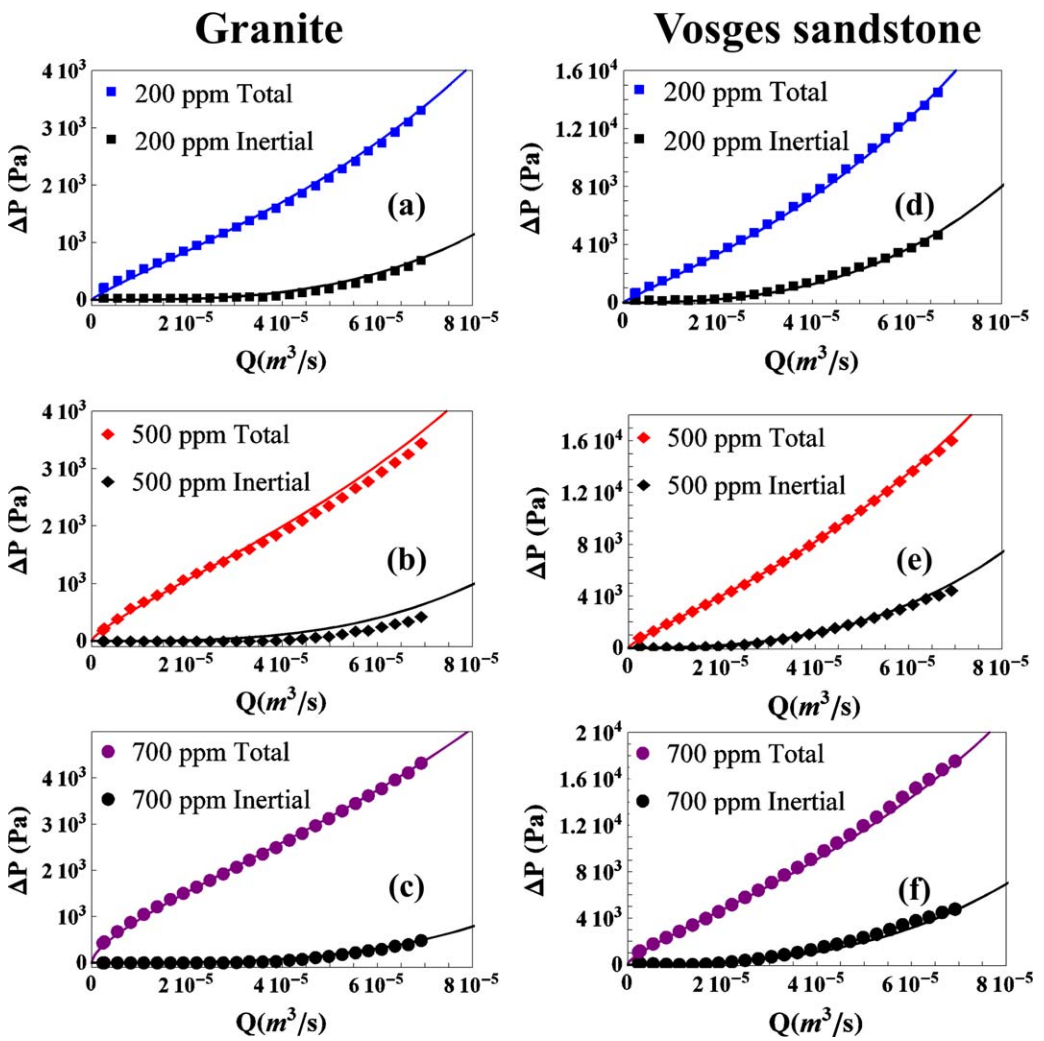

Figure 7. Total and Inertial pressure losses as a function of Q corresponding to (a,b,c,d) Granite and (e,f,g,h) Vosges sandstone fractures. Symbols represent experimental data and solid lines represent predictions using β and γ obtained from water injection.

The values of β and γ obtained from water injection (Table 2) were used for all the injected fluids, independently of C_p to predict ΔP_{total} and $\Delta P_{inertial}$. These predictions are represented in Figure 7 (solid lines) together with the experimental results (symbols). It is noticed that predictions are in good agreement with experiments both for the total and the inertial pressure differences.

5. Discussion

As can be observed in Figure 2, the $(Q_i, \nabla P_i,)$ data corresponding to the granite fracture are well fitted by a weak inertia cubic law, as the deviations from linearity follow a cubic function of Q with no quadratic contribution. Therefore, it can be deduced that viscous effects dominate the flow at the lowest Q ($Q < 3 \times 10^{-5}$ m^3/s) and extra pressure losses due to cross viscous-inertia effects become important at moderate and high flow rates. In the case of the Vosges sandstone fracture, these deviations are not fully described by the cubic term and an additional quadratic term (full cubic law) is needed to correctly fit the experimental data. From these observations, it can be deduced that a weak inertia regime dominates the flow of water through the granite fracture while a transition from weak to strong inertial regime where cross viscous-inertia effects are significant occurs in the case of the Vosges sandstone fracture.

Figure 3 shows that equivalent viscosity undergoes a drop in value corresponding to shear-thinning Darcy regime followed by an increase in the inertial regime. This is in good agreement with the numerical

experiments conducted by *Tosco et al.* [2013] and applies for all values of C_p. It is highlighted that the inertial regime occurs at high flow rates that lie in the region close to the upper Newtonian plateau of viscosity where the shear-thinning behavior is moderate. Also, μ_{pm} is higher for polymer solution injection in granite fracture than in Vosges sandstone fracture. This was expected given the lower shear rates experienced by the fluid in the most permeable fracture. In contrast, the values of μ_{eq} corresponding to the high shear flow region are very close in both fractures. Also, the differences between μ_{eq} and μ_{pm} are more important in the case of Vosges sandstone because of the existence of quadratic inertial pressure losses.

The range of variation of μ_{eq} increases as C_p increases for both fractures. This is a consequence of the higher degree of shear-thinning presented by the most concentrated solutions as shown in Figure 1. Besides, the range of variation of μ_{eq} is wider for the granite than for the Vosges sandstone fracture. This is due to the higher shear rates to which the fluid is subjected during its flow through the granite Vosges fracture. Indeed, these higher shear rates lie in the region close to the upper Newtonian plateau viscosity where the shear-thinning behavior is less significant. It is also observed that the difference between μ_{eq} and μ_{pm} is more pronounced in the case of the Vosges sandstone fracture for all considered values of C_p. Moreover, stronger differences between μ_{eq} and μ_{pm} were found at the lowest polymer concentration for the granite fracture while this difference remains approximately constant at all concentrations for the Vosges sandstone fracture. This implies that polymer solution injection is more efficient for reducing the relative importance of inertial pressure losses in the case of the most permeable fracture (granite fracture).

Figure 4 shows that while Reynolds number is a linear function of Q for $C_p = 0$ ppm, this is not the case for higher concentrations due to the extra increase in Reynolds number arising from shear-thinning behavior. However, deviations from linearity are less marked for the Vosges sandstone fracture. This is a consequence of the higher shear rates generated by the smaller apertures of this fracture, which lie in the region close to the upper Newtonian plateau viscosity where the shear-thinning behavior is less significant as presented in the preceding subsection.

The measured pressure losses were higher in the case of the most permeable fracture (Vosges sandstone) as can be observed in Figure 5. One can remark that, in contrast to Newtonian fluids, the shear contributions of shear-thinning fluids ($C_p > 0$) are not linear with Reynolds number as expected from the rheograms presented in Figure 1. It is remarked that ΔP_{shear} is always higher than $\Delta P_{inertial}$ within the investigated range of Reynolds numbers. In particular, $\Delta w_{inertial}$ is less important in the case of the granite fracture, which is coherent with the weaker inertial regime (cubic law) obtained in subsection 3.1. Besides, $\Delta P_{inertial}$ are lower as C_p increases, due to the lower values of Reynolds number.

It is remarked in Figure 6 that the range of critical Reynolds number is narrow for both fractures (0.25–0.34 for granite and 0.037–0.058 for Vosges sandstone), showing no decisive effect of C_p within the investigated range.

From equations (2) and (3), $\Delta(_{total}$ can be expressed as follows:

$$-\Delta P_{total} = \frac{\mu}{K}\frac{Q}{A}L\left(1+Re_c^2\right) \tag{16}$$

Therefore, the critical Reynolds number predicted by cubic law must satisfy the condition $\Delta h_{inertial}/\Delta n_{total} = Re_c^* 2/\left(1+Re_c^* 2\right) = 0.05$, which gives $Re_c^* = 0.23$.

In the transitional inertia regime Δn_{total} can be expressed, from equations (4) and (5), as:

$$-\Delta P_{total} = \frac{\mu}{K}\frac{Q}{A}L\left(1+Re_{fc}+\frac{\gamma}{K\beta^2}Re_{fc}^2\right) \tag{17}$$

In this case, the critical Reynolds number predicted by full cubic law must satisfy the condition $\Delta P_{inertial}/\Delta P_{total} = \left(Re_{fc}^* + \frac{\gamma}{K\beta^2}Re_{fc}^* 2\right)/\left(1+Re_{fc}^* + \frac{\gamma}{K\beta^2}Re_{fc}^* 2\right) = 0.05$. Assuming that the values of β and γ obtained for water apply to all considered C_p, a value of $Re_{fc}^* = 0.037$ is obtained. This value is very close to those experimentally determined, which is coherent with uniqueness of inertial coefficients for a given porous medium independently of the injected fluid [*Hayes et al.*, 1996; *Tosco et al.*, 2013]. It should be noted that according to both cubic and full cubic laws, the onset of inertial effects occurs at $Re_c = 0$, which is not realistic. Consequently, a nonzero inertial pressure loss is predicted at the actual onset of inertial effects. This explains that the obtained values for the critical Reynold numbers are slightly higher than predicted.

The results and comparison presented in Figure 7 prove that, within the range of porous media and fluids investigated in this work, β and γ do not depend on the rheology of the injected fluid. Therefore, when compared to Newtonian fluids, only the aditional empirical parameter α is needed to predict the relations between pressure drop and flow rate during the inertial flow of shear-thinning fluids in fractures. However, α can be determined through noninertial flow experiments in the studied porous medium. Consequently, the pressure losses generated at high flow rates, where inertial effects are important, can be predicted from (1) the results of shear-thinning Darcian flow experiments (determination of α) and (2) Newtonian flow experiments (determination of β and γ) in the investigated porous medium.

6. Summary and Conclusions

Motivated by the wide range of industrial applications in which understanding non-Darcian flow of shear-thinning fluids is of key importance, we have investigated the effects of the shear rheology of the injected fluid on the pressure losses generated during flow through fractures. To do so, we have conducted a series of single-phase flow experiments injecting aqueous solutions of xanthan biopolymer with different polymer concentration through two replicas of rough-walled natural fractures (granite and Vosges sandstone).

K, γ, and β were determined for both fractures from water flow experiments by means of a rigorous procedure, showing that different inertia regimes occur in each fracture (weak inertia regime for granite, transitional inertia regime for Vosges sandstone). In both cases, cubic and full cubic law proved to fit very well the experimental data. Also, the importance of inertial effects in the porous medium was quantified through comparison of the calculated shear viscosity to the equivalent viscosity observed in the fractures. Indeed, μ_{eq} was shown to undergo a drop in value within the shear-thinning Darcy regime followed by an increase in the inertial regime, in good agreement with previous numerical experiments [*Tosco et al.*, 2013]. These results were extended to all tested values of C_p. Stronger differences between μ_{eq} and μ_{pm} were found at the lowest polymer concentration for the granite fracture while this difference remains approximately constant at all concentrations for the Vosges sandstone fracture, showing that adding polymer is more efficient for reducing the relative importance of inertial pressure losses in the case of the most permeable fracture (granite).

The effects of C_p on Reynolds number were assessed, showing nonlinearity of Reynolds number versus Q for shear-thinning fluids and finding lower values and narrower ranges of variation of Reynolds number for high values of C_p. Moreover, deviations from linearity were found to be less marked for the Vosges sandstone fracture. This is attributed to the higher shear rates generated by the smaller apertures of this fracture, which lie in the region close to the upper Newtonian plateau viscosity where the shear-thinning behavior is less significant.

For the first time, inertial and shear contributions to pressure loss have been identified for the flow of shear-thinning fluids in fractures. $\Delta P_{inertial}$ and ΔP_{shear} were calculated and presented as a function of Reynolds number and C_p for both fractures. $\Delta P_{inertial}$ is less important in the case of the granite fracture, given the weaker inertial regime (cubic law). Besides, the inertial pressure losses are lower as C_p increases, due to the reduction in Reynolds number values. No significant dependence between C_p and the onset of inertial effects was observed. However, the obtained values for the critical Reynolds number were slightly higher than those predicted by the cubic and the full-cubic laws. This is explained by the unrealistic inertial effects introduced by both laws at low values of Reynolds numbers.

The values of β and γ obtained from water injection were used to predict ΔP_{total} and $\Delta P_{inertial}$ for all the injected fluids, independently of C_p. The obtained results were in good agreement with experiments both for the total and the inertial pressure differences, proving that, within the range of porous media and fluids investigated in this work, β and γ do not depend on the rheology of the injected fluid. Therefore, when compared to Newtonian fluids, only the aditional empirical parameter α is needed to predict the relations between pressure drop and flow rate during the inertial flow of shear-thinning fluids in fractures. However, α can be determined through noninertial flow experiments in the studied porous medium. Consequently, the pressure losses generated at high flow rates, where inertial effects are important, can be predicted from (1) the results of shear-thinning Darcian flow experiments (determination of α) and (2) Newtonian flow experiments (determination of K, β, and γ) in the investigated porous medium. As an alternative, if the pore-level structure of the medium is known sufficiently in detail (e.g., from 3-D microtomography imaging),

α, β, γ, and K can be determined from the expressions presented in the literature [*Cornell and Katz*, 1953; *Geertsma*, 1974; *Neasham*, 1977; *Noman and Archer*, 1987; *Agnaou et al*., 2013; *Agnaou*, 2014] or from 2-D or 3-D pore-scale flow simulations following the procedure proposed by *Tosco et al*. [2013]. Besides, the influence of α on $\Delta P_{inertial}$ has been shown to be weak in our experiments as the involved shear rates are close to the upper Newtonian plateau of viscosity.

The experimental results presented in this paper enabled us to validate, adapt, and extend available macroscopic flow equations to the case of shear-thinning fluids. Moreover, previous theoretical [*Hayes et al*., 1996] and numerical [*Tosco et al*., 2013] results stating uniqueness of inertial coefficients for a given porous media have been experimentally tested and validated. We have now demonstrated the uniqueness of β for all tested polymer concentration. Also, our hypothesis that the differences between ΔP_{total} and ΔP_{shear} can be explained in terms of inertial effects has been validated, as no evidence of extra pressure drop arising from elongational viscosity was found. Therefore, it has been proved that the apparent shear-thickening observed during flow of polymer solutions at high flow rates, which is usually attributed to elongational flow dissipation, can be explained in terms of inertial dissipation in the present experiments. This may the consequence of the minor geometrical complexity of fractures as compared to that of most granular porous media. However, only weak and transitional inertia regimes were explored in our experiments, so important elongational effects are not dismissed at higher flow rates and polymer concentrations. Indeed, porous media flow was turbulent in some previous works reporting extension-thickening [*Amundarain et al*., 2009].

Also, these results may provide useful guidance for the selection of the polymer concentration and the injection flow rate when injecting aqueous polymer solutions. In particular, the obtained relationships can be implemented in chemical flood simulation software for soil remediation and EOR so as to provide a more realistic alternative to the Newtonian assumption allowing a better prediction of Q versus Δs at the pilot plant and reservoir scales. The results of this work should now be extended to stronger inertia regimes and to other types of porous media with different permeability and more complex internal geometries than fractures, where elongational effects may be observed.

Acknowledgments
The authors would like to thank Frédéric Bastien for his assistance with the experimental setup. Supporting data are included as three figures in SI files; any additional data may be obtained from the authors (antonio.rodriguezdecastro@ensam.eu).

References

Agnaou, M (2014), Une étude numérique des écoulements mono et diphasique inertiels en milieux poreux, PhD thesis, Arts et Métiers ParisTech, Courbevoie.

Agnaou, M., D. Lasseux, and A. Ahmadi (2013), Simulations d'écoulements inertiels en milieu poreux, in *21ème CFM*, AFM, Courbevoie, France.

Amaral Souto, H., and C. Moyne (1997), Dispersion in two-dimensional periodic porous media, Part I. Hydrodynamics, *Phys, Fluids*, *9*(8), 2243–2252.

Amundarain, J. L., L. J. Castro, M. R. Rojas, S. Siquier, N. Ramírez, A. J. Müller, and A. E. Sáez (2009), Solutions of xanthan gum/guar gum mixtures: Shear rheology, porous media flow, and solids transport in annular flow, *Rheol. Acta 48*, 491–498.

Auradou, H., A. Boschan, R. Chertcoff, S. Gabbanelli, J. P. Hulin, and I. Ippolito (2008), Enhancement of velocity contrasts by shear-thinning solutions flowing in a rough fracture, *J. Nonnewton. Fluid Mech*., *153*, 53–61.

Barrère, J. (1990), Modélisation des écoulements de Stokes et Navier-Stokes en milieu poreux, PhD thesis, Univ. of Bordeaux, Bordeaux, France.

Bird, R. B., R. C. Armstrong, and O. Hassager (1987), *Dynamics of Polymeric Liquids vol. 1: Fluid Dynamics*, 2nd ed., John Wiley, New York.

Brown, S. R. (1987), Fluid flow through rock joints: The effect of surface roughness, *J. Geophys. Res. 92*(B2), 1337–1347, doi:10.1029/JB092iB02p01337.

Brush, D. J., and N. R. Thomson (2003), Fluid flow in synthetic rough walled fractures: Navier–Stokes, Stokes, and local cubic law simulations, *Water Resour. Res. 39*(4), 1085, doi:10.1029/2002WR001346.

Buès, M., M. Panfilov, and C. Oltean (2004), Macroscale model and inertia-viscous effects for Navier–Stokes flow in a radial fracture with corrugated walls, *J. Fluid Mech*., *504*, 41–60, doi:10.1017/S002211200400816X

Carreau, P. J. (1972), Rheological equations from molecular network theories, *Trans. Soc. Rheol*., *16*, 99–127.

Chauveteau, G. (1982), Rodlike polymer solution flow through fine pores: Influence of pore size on rheological behavior, *J. Rheol*., *26*, 111.

Chauveteau, G., and C. Thirriot (1967), Régimes d'écoulement en milieu poreux et limite de la loi de Darcy, *La Houille Blanche*, *2*, 141–148. doi:10.1051/lhb/1967009.

Chen, Z., S. L. Lyons, and G. Qin (2001), Derivation of the Forchheimer law via homogenization, *Transp. Porous Media*, *44*(2), 325–335, doi:10.1023/A:1010749114251.

Collier, J. R., S. Petrovan, N. Hudson, and X. Wei (2007), Elongational rheology by different methods and orientation number, *J. Appl. Polym. Sci*., *105*, 3551–3561, doi:10.1002/app.26413.

Comba, S., D. Dalmazzo, E. Santagata, and R. Sethi (2011), Rheological characterization of xanthan suspensions of nanoscale iron for injection in porous media, *J. Hazard. Mater*., *185*, 598–605.

Cornell, D., and D. L. Katz (1953), Flow of gases through consolidated porous media, *Ind. Eng. Chem*., *45*(10), 2145–2153, doi:10.1021/ie50526a021.

Cvetkovic, V. D. (1986), A continuum approach to high velocity flow in a porous medium, *Transp. Porous Media*, *1*(1), 63–97, doi:10.1007/BF01036526.

Darcy, H. J. (1856), *Les Fontaines Publiques de la Vue de Dijon*, pp. 590–594, Libraire de Corps Impériaux des Ponts et Chausées et des Mines, Paris.
Dukhan, N., Ö. Bağcı, and M. Özdemir (2014), Experimental flow in various porous media and reconciliation of Forchheimer and Ergun relations, *Exp. Therm. Fluid Sci.*, *57*, 425–433, doi:10.1016/j.expthermflusci.2014.06.011.
Dullien, A. L., and M. I. S. Azzam (1973), Flow rate-pressure gradient measurement in periodically nonuniform capillary tube, *AIChE J.*, *19*, 222–229, doi:10.1002/aic.690190204.
Du Plessis, J. E., and J. H. Masliyah, (1988), Mathematical modeling of flow through consolidated isotropic porous media, *Trans. Porous Media*, *3*, 145–161, doi:10.1007/BF00820342.
Fang, J., T. Zhu, J. Sheng, Z. Jiang, and Y. Ma (2015), Thickness dependent effective viscosity of a polymer solution near an interface probed by a quartz crystal microbalance with dissipation method, *Sci. Rep.*, *5*, 8491, doi:10.1038/srep08491.
Firdaouss, M, and J. L. Guermond (1995), Sur l'homogénéisation des équations de Navier-Stokes à faible nombre de Reynolds, *C. R. Acad. Sci. Paris*, *320*, 245–251.
Firdaouss, M., J.-L. Guermond, and P. Le-quéré (1997), Nonlinear correction to Darcy's law at low Reynolds numbers, *J. Fluid Mech.*, *343*, 331–350, doi:10.1017/S0022112097005843.
Forchheimer, P. (1901), Wasserberwegng durch Boden, *Forschtlft ver. D. Ing.*, *45*(50), 1782–1788.
Fourar, M., G. Radilla, R. Lenormand, and C. Moyne (2004), On the non-linear behavior of a laminar single-phase flow through two and three-dimensional porous media, *Adv. Water Resour.*, *27*(6), 669–677, doi:10.1016/j.advwatres.2004.02.021.
Garcia-Ochoa, F., V. E. Santosa, J. A Casasb, and E. Gómez (2000), Xanthan gum: Production, recovery, and properties, *Biotechnol. Adv.*, *18*, 549–579.
Geertsma, M. (1974), Estimating the coefficient of inertial resistance fluid flow through porous media, *Soc. Pet. Eng. J.*, *14*(5), 445–450, doi: 10.2118/4706-PA.
Giorgi, T. (1997), Derivation of the Forchheimer law via matched asymptotic expansions, *Transp. Porous Media*, *29*(2), 191–206, doi:10.1023/A:1006533931383.
González, J. M., A. J. Müller, M. F. Torres, and A. E. Sáez (2005), The role of shear and elongation in the flow of solutions of semi-flexible polymers through porous media, *Rheol. Acta*, *44*, 396–405, doi:10.1007/s00397-004-0421-4.
Hallouche, M. H., V. Botton, D. Henry, S. Millet, R. Usha, and H. Ben Hadid (2015), Experimental determination of the viscosity at very low shear rate for shear thinning fluids by electrocapillarity, *J. Nonnewton. Fluid Mech.*, *215*, 60–69.
Hayes, R. E., A. Afacan, B. Boulanger, and A. V. Shenoy (1996), Modelling the flow of power law fluids in a packed bed using a volume-averaged equation of motion, *Transp. Porous Media*, *23*(2), 175–196, doi:10.1007/bf00178125.
Hernández-Espriú, A., E. Sánchez-León, P. Martínez-Santos, and L. G. Torres (2013), Remediation of a diesel-contaminated soil from a pipeline accidental spill: Enhanced biodegradation and soil washing processes using natural gums and surfactants, *J. Soils Sediment.*, *13*, 152–165.
Hubbert, M. K. (1956), Darcy law and the field equations of the flow of underground fluids, *Trans. Am. Inst. Min. Metall. Eng. 207*, 222–239.
Isakov, E., S. R. Ogilvie, C. W. Taylor, and P. W. J. Glover (2001), Fluid flow through rough fractures in rocks I: High resolution aperture determinations, *Earth Planet. Sci. Lett.*, *191*(3–4), 267–282, doi:10.1016/S0012-821X(01)00424-1.
Javadi, M., M. Sharifzadeh, and K. Shahriar (2010), A new geometrical model for non-linear fluid flow through rough fractures, *J. Hydrol.*, *389*, 18–30, doi:10.1016/j.jhydrol.2010.05.010.
Lavrov, A. (2015), Flow of truncated power-law fluid between parallel walls for hydraulic fracturing applications, *J. Nonnewton. Fluid Mech.*, *223*, 141–146.
López, X. (2004), *Pore-Scale Modelling of Non-Newtonian Flow*, PhD thesis, Dep. Earth Sci. & Eng. Pet. Eng. & Rock Mech. Group, Imp. Coll., London, U. K.
López, X., P. H. Valvatne, and M. J. Blunt (2003), Predictive network modeling of single-phase non-Newtonian flow in porous media, *J. Colloid Interface Sci.*, *264*(1), 256–265, doi:10.1016/s0021-9797(03)00310-2.
MacDonald, I. F., M. S. El-Sayed, K. Mow, and F. A. L. Dullien (1979), Flow through porous media, the Ergun equation revisited, *Ind. Eng. Chem. Fundam.*, *18*(3), 199–208, doi:10.1021/i160071a001.
Mei, C. C., and J. -L. Auriault (1991), The effect of weak inertia on flow through a porous medium, *J. Fluid Mech.*, *222*, 647–663, doi:10.1017/S0022112091001258.
Miskimins, J. L., H. D. Lopez-Hernandez, and R. D. Barree (2005), Non-Darcy flow in hydraulic fractures: Does it really matter?, paper SPE 96389 Annual Technical Conference and Exhibition, Soc. of Pet. Eng., Dallas, Tex., 9–12 Oct.
Mongruel, A., and M. Cloitre (2003), Axisymmetric orifice flow for measuring the elongational viscosity of semi-rigid polymer solutions, *J. Nonnewton. Fluid Mech.*, *110*, 27–43.
Müller A. J., and A. E. Sáez (1999), The rheology of polymer solutions in porous media, in *Flexible Polymer Chain Dynamics in Elongational Flow: Theory and Experiment*, edited by T. Q. Nguyen and H. H. Kausch, pp. 335–393, Springer, Heidelberg.
Neasham, J. W. (1977), The morphology of dispersed clay in sandstone reservoirs and its effects on sandstone shaliness, pore space and fluid flow properties, paper SPE 6858 presented at the 1977 SPE Annual Technical Conference and Exhibition, Soc. of Pet. Eng., Denver, Colo., doi:10.2118/6858-MS.
Nguyen, T. Q., and H. H. Kausch (1999), *Flexible Polymer Chains in Elongational Flow: Theory and Experiement*, Springer, Berlin.
Noman, R., and M. S. Archer (1987), The effect of pore structure on Non-Darcy gas flow in some low permeability reservoir rocks, paper SPE 16400 presented at the SPE/DOE Low Permeability Reservoirs Symposium, Soc. of Pet. Eng., Denver, Colo., doi:10.2118/16400-MS.
Nowamooz, A., G. Radilla, M. Fourar, and B. Berkowitz (2013), Non-Fickian transport in transparent replicas of rough-walled rock fractures, *Transp. Porous Media*, *98*, 651–682, doi:10.1007/s11242-013-0165-7.
Palaniraj, A., and V. Jayaraman (2011), Production, recovery and applications of xanthan gum by Xanthomonas campestris, *J. Food Eng.*, *106*, 1–12.
Panfilov, M., and M. Fourar (2006), Physical splitting of nonlinear effects in high-velocity stable flow through porous media, *Adv. Water Resour.*, *29*, 30–41.
Pauchard, L., F. Varela López, M. Rosen, C. Allain, P. Perrot, and M. Rabaud (1999), On the effects of Non-Newtonian fluids above the ribbing instability, in *Proceedings of Advances in Coating and Drying of Thin Films*, Shaker, Aachen, pp. 183–188.
Perrin, C. L., P. M. J. Tardy, K. S. Sorbie, and J. C. Crawshaw (2006), Experimental and modeling study of Newtonian and non-Newtonian fluid flow in pore network micromodels, *J.Colloid Interface Sci.*, *295*(2), 542–550, doi:10.1016/j.jcis.2005.09.012.
Perkowska M, G. Mishuris, and M. Wrobel (2016), Universal hydrofracturing algorithm for shear-thinning fluids: Particle velocity based simulation, *Comput. Geotech.*, *71*, 310–37.
Petrie, C. J. S. (2006), Extensional viscosity: A critical discussion, *J. Nonnewton. Fluid Mech*, *137*, 15–23.

Radilla, G., A. Nowamooz, and M. Fourar (2013), Modeling Non-Darcian single- and two-phase flow in transparent replicas of rough-walled rock fractures, *Transp. Porous Media*, *98*, 401–426, doi:10.1007/s11242-013-0150-1.
Rasoloarijaona, M., and J. L. Auriault (1994), Nonlinear seepage flow through a rigid porous medium, *Eur. J. Mech. B Fluids*, *13*(2), 177–195.
Rocha, R. P. A., and M. E. Cruz (2010), Calculation of the permeability and apparent permeability of three-dimensional porous media, *Transp. Porous Media*, *83*(2), 349–373, doi:10.1007/s11242-009-9445-7.
Rodríguez S, C. Romero, M. L. Sargenti, A. J. Müller, A. E. Sáez, and J. A. Odell (1993), Flow of polymer solutions through porous media, *J Nonnewton. Fluid Mech*, *49*, 63–85.
Rodríguez de Castro, A. (2014), Flow experiments of yield stress fluids in porous media as a new porosimetry method, PhD thesis, Arts et Métiers ParisTech, Paris, France. [Avaialble at https://pastel.archives-ouvertes.fr/file/index/docid/1068908/filename/RODRIGUEZ_-_DE_-_CASTRO.pdf/.]
Rodríguez de Castro, A., A. Omari, A. Ahmadi-Sénichault, and D. Bruneau (2014), *Transp. Porous Media*, *101*(3), 349–364.
Rodríguez de Castro, A., M. Oostrom, and N. Shokri (2016), Effects of shear-thinning fluids on residual oil formation in microfluidic pore networks, *J. Colloid Interface Sci.*, *472*, 34–43, doi:10.1016/j.jcis.2016.03.027.
Saggin, R., and J. N. Coupland (2004), Rheology of xanthan/sucrose mixtures at ultrasonic frequencies, *J. Food Eng.*, *65*, 49–53.
Scheidegger, A. E. (1960), *The Physics of Flow Through Porous Media*, Macmillan, New York.
Schneebeli, G. (1955), Expériences sur la limite de validité de la loi de Darcy et l'apparition de la turbulence dans un écoulement de filtration. *La Houille Blanche 2*, 141–149. doi:10.1051/lhb/1955030.
Schunk, P. R., J. M. de Santos, and L. E. Scriven (1990), Flow of Newtonian liquids in opposed-nozzles configuration, *J. Rheol.*, *34*, 387–414.
Seright, R. S., T. Fan, K. Wavrik, and R. de Carvalho Balaban (2011), New insights into polymer rheology in porous media, *SPE J.*, *16*, 35–42, doi:10.2118/129200-PA.
Silva, J. A. K., M. Smith, J. Munakata-Marr, and J. E. McCray (2012), The effect of system variables on in situ sweep-efficiency improvement via viscosity modification, *J. Contam. Hydrol. 136*, 117–130.
Song, Y. -Q. (2007), Novel NMR techniques for porous media research, *Cem. Concr. Res.*, *37*, 325–328.
Sorbie, K. S., P. J. Clifford, and E. R. W. Jones, (1989), The rheology of pseudoplastic fluids in porous media using network modeling, *J. Colloid Interface Sci.*, *130*(2), 508–534.
Sorbie, K. S., P. J. Clifford, and E. R. W. Jones (2013), The rheology of pseudoplastic fluids in porous media using network modeling, *J. Colloid Interface Sci.*, *130*(2), 508–534.
Tosco, T., D. L. Marchisio, F. Lince, and R. Sethi (2013), Extension of the Darcy–Forchheimer law for shear-thinning fluids and validation via pore-scale flow simulations, *Transp. Porous Media*, *96*, 1–20, doi:10.1007/s11242-012-0070-5.
Truex, M., et al. (2015), Field test of enhanced remedial amendment delivery using a shear-thinning fluid, *Ground Water Monit. Rem.*, *35*, 34–45, doi: 10.1111/gwmr.12101.
Wadhai, V. S., and A. N. Dixit (2011), Production of Xanthan gum by *Xanthomonas campestris* and comparative study of Xanthomonas campestris isolates for the selection of potential Xanthan producer, *Indian Streams Res. J. 1*, 1–4.
Wengeler, L. (2014), *Coating and Drying Processes for Functional Films in Polymer Solar Cells: From Laboratory to Pilot Scale*, KIT Sci. Publ., Karlsruhe.
Willenbacher, N., and R. Hingmann (1994), Shear and elongational flow properties of fluid S1 from rotational, capillary, and opposed jet rheometry, *J. Nonnewton. Fluid Mech.*, *52*, 163–176.
Witherspoon, P.A., J. S. Y. Wang, K. Iwai, and J. E. Gale (1980), Validity of cubic law for fluid flow in a deformable rock fracture, *Water Resour. Res.*, *16*(6), 1016–1024, doi:10.1029/WR016i006p01016.
Wodie, J. C., and T. Levy (1991), Correction non linéaire de la loi de Darcy, *C. R. Acad. Sci. Paris*, *312*, 157–161.
Yazdchi, K., and S. Luding (2012), Towards unified drag laws for inertial flow through fibrous materials, *Chem. Eng. J.*, *207–208*, 35–48.
Zeng, Z., and R. Grigg (2006), A criterion for non-Darcy flow in porous media, *Transp. Porous Media*, *63*(1), 57–69.
Zhang, L., H. Sun, B. Han, L. Peng, F. Ning, G. Jiang, and V. F. Chehotkin (2016), Effect of shearing actions on the rheological properties and mesostructures of CMC, PVP and CMC + PVP aqueous solutions as simple water-based drilling fluids for gas hydrate drilling, *J. Unconvent. Oil Gas Resour.*, *14*, 86–98.
Zhong, L., M. Oostrom, T. W. Wietsma, and M. A. Covert (2008), Enhanced remedial amendment delivery through fluid viscosity modifications: Experiments and numerical simulations, *J. Contam. Hydrol.*, *101*, 29–41, doi:10.1016/j.jconhyd.2008.07.007.
Zimmerman, R. W., and I. W. Yeo (2000), Fluid flow in rock fractures: From the Navier–Stokes equations to the cubic law, in *Dynamics of Fluids in Fractured Rock, Geophys. Monogr. Ser.* vol. 122, edited by B. Faybishenko, P. A. Witherspoon, and S. M. Benton, pp. 213–224. AGU, Washington, D. C.
Zimmerman, R. W., A. H. Al-Yaarubi, C. S. Pain, and C. A. Grattoni (2004), Nonlinear regimes of fluid flow in rock fractures, *Int. J. Rock Mech. Min. Sci.*, *41*, 163.